Inorg. Chem. **2004**, *43*, 2141–2150

Mechanistic Studies on the Formation and Reactivity of Dioxygen Adducts of Diiron Complexes Supported by Sterically Hindered Carboxylates

Sergey V. Kryatov,[†] Ferman A. Chavez,[‡] Anne M. Reynolds,[‡] Elena V. Rybak-Akimova,*[,†] Lawrence Que, Jr.,*[,‡] and William B. Tolman*[,‡]

Department of Chemistry, Tufts University, 62 Talbot Avenue, Medford, Massachusetts 02155, and Department of Chemistry and Center for Metals in Biocatalysis, University of Minnesota, 207 Pleasant Street SE, Minneapolis, Minnesota 55455

Received January 2, 2004

Dioxygen activation by enzymes such as methane monooxygenase, ribonucleotide reductase, and fatty acid desaturases occurs at a nonheme diiron active site supported by two histidines and four carboxylates, typically involving a (peroxo)diiron(III,III) intermediate in an early step of the catalytic cycle. Biomimetic tetracarboxylatodiiron(II,II) complexes with the familiar "paddlewheel" topology comprising sterically bulky *o*-dixylylbenzoate ligands with pyridine, 1-methylimidazole, or THF at apical sites readily react with O_2 to afford thermally labile peroxo intermediates that can be trapped and characterized spectroscopically at low temperatures (193 K). Cryogenic stopped-flow kinetic analysis of O_2 adduct formation carried out for the three complexes reveals that dioxygen binds to the diiron(II,II) center with concentration dependences and activation parameters indicative of a direct associative pathway. The pyridine and 1-methylimidazole intermediates decay by self-decomposition. However, the THF intermediate decays much faster by oxygen transfer to added PPh_3, the kinetics of which has been studied with double mixing experiments in a cryogenic stopped-flow apparatus. The results show that the decay of the THF intermediate is kinetically controlled by the dissociation of a THF ligand, a conclusion supported by the observation of saturation kinetic behavior with respect to PPh_3, inhibition by added THF, and invariant saturation rate constants for the oxidation of various phosphines. It is proposed that the proximity of the reducing substrate to the peroxide ligand on the diiron coordination sphere facilitates the oxygen-atom transfer. This unique investigation of the reaction of an O_2 adduct of a biomimetic tetracarboxylatodiiron(II,II) complex provides a synthetic precedent for understanding the electrophilic reactivity of like adducts in the active sties of nonheme diiron enzymes.

Introduction

A (peroxo)diiron(III,III) intermediate supported by a ligand set comprising 4 carboxylates and 2 histidine imidazoles plays a central role in the catalytic mechanisms of nonheme diiron enzymes such as methane monooxygenase (MMO), ribonucleotide reductase (RNR), and fatty acid desaturases.[1−4] Formed through the reaction of the reduced, diiron(II,II) form of the enzymes with O_2, this intermediate undergoes O−O bond scission and converts to various high valent species that are deemed responsible for attacking substrate.[1,5] Evidence for the capability of the (peroxo)diiron(III,III) unit to functionalize certain substrates also has been presented,[6] suggesting intriguing analogies to the "two oxidant" hypothesis under consideration for heme-iron oxygenases.[7] In complementary and synergistic efforts to understand the

* To whom correspondence should be addressed. E-mail: erybakak@tufts.edu (E.V.R.-A.); que@chem.umn.edu (L.Q.); tolman@chem.umn.edu (W.B.T.). Fax: (617) 627-3443 (E.V.R.-A.); (612) 624-7029 (L.Q. and W.B.T.).

[†] Tufts University.

[‡] University of Minnesota.

(1) Wallar, B. J.; Lipscomb, J. D. *Chem. Rev.* **1996**, *96*, 2625−2658.
(2) Solomon, E. I.; Brunold, T. C.; Davis, M. I.; Kemsley, J. N.; Lee, S.-K.; Lehnert, N.; Neese, F.; Skulan, A. J.; Yang, Y.-S.; Zhou, J. *Chem. Rev.* **2000**, *100*, 235−349.
(3) Merkx, M.; Kopp, D. A.; Sazinsky, M. H.; Blazyk, J. L.; Müller, J.; Lippard, S. J. *Angew. Chem., Int. Ed.* **2001**, *40*, 2782−2807.
(4) Friesner, R. A.; Baik, M.-H.; Gherman, B. F.; Guallar, V.; Wirstam, M.; Murphy, R. B.; Lippard, S. J. *Coord. Chem. Rev.* **2003**, *238*−*239*, 267−290.
(5) Baik, M.-H.; Newcomb, M.; Friesner, R. A.; Lippard, S. J. *Chem. Rev.* **2003**, *103*, 2385−2419.
(6) Valentine, A. M.; Stahl, S. S.; Lippard, S. J. *J. Am. Chem. Soc.* **1999**, *121*, 3876−3887.

10.1021/ic049976t CCC: $27.50
Published on Web 02/20/2004

nature of the reactive intermediates in the diiron enzymes, synthetic peroxo and high valent diiron complexes have been targeted for detailed characterization.[8−11] The reactions of diiron(II,II) compounds with O_2 are of particular interest for providing insight into the initial steps of dioxygen activation by the biological systems, and several structurally defined (peroxo)diiron(III,III) species have been prepared via this route.[11−15] Kinetic and thermodynamic data with which to evaluate the mechanisms of formation, decomposition, and/or reactivity with added substrates of such species have been obtained in a few cases.[16−24] Such mechanistic understanding is limited, however, particularly for systems that feature a biomimetic tetracarboxylate supporting ligand set and involve reactions of well-defined (peroxo)diiron(III,III) species with exogenous substrates.[21,23]

A fruitful strategy for the construction of reactive diiron complexes that closely model the diiron protein active sites involves the use of bulky carboxylate ligands, which have enabled the isolation of a variety of structural motifs through hydrophobic shielding and interligand steric interactions.[9,24,25] In a recent communication,[26] we reported the use of the dixylyl-carboxylate **A** for the synthesis of the series of diiron(II,II) complexes **1** that feature the familiar tetracarboxylate "paddlewheel" topology (Scheme 1). Oxygenation of these complexes at low temperature (193 K) yields species **2**, which were postulated to be (peroxo)diiron(III,III) complexes on the basis of resonance Raman, Mössbauer, and EPR

Scheme 1

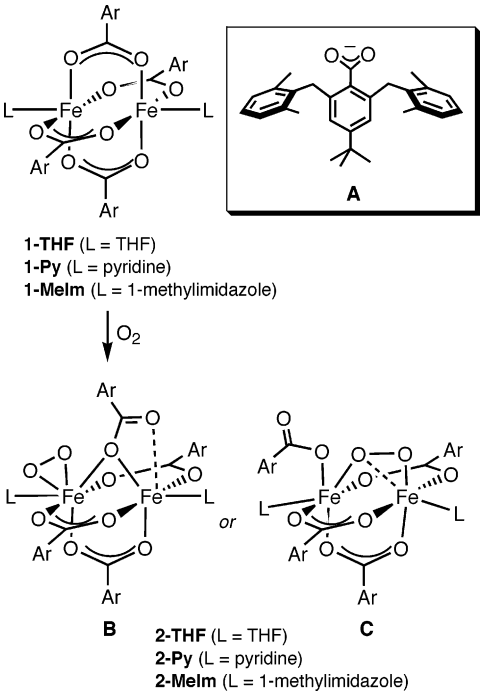

spectroscopic data. The specific structural proposal **B** shown for **2** (Scheme 1) is consistent with the observation of (a) a $\nu_{OO} = 822$ cm^{-1} that is lower than typical for μ-1,2-peroxo complexes[11,27] and is in the range observed for monoiron η^2-peroxo compounds,[11,28] and (b) Mössbauer spectra that indicate inequivalent ferric sites, one with a high $\delta = 0.65(2)$ mm s^{-1} generally characteristic of Fe(III) coordinated to peroxide,[26] and which are only weakly antiferromagnetically coupled ($J \approx 30(5)$ cm^{-1}; $H = JS_1 \cdot S_2$). The data are not unambiguous, however, and an alternative formulation **C** could not be excluded. While efforts to more fully characterize the structures of **2** continue, we have begun to explore the reactivity of these complexes, and we report herein the results of rapid kinetic studies of the oxygenation of **1** to yield **2** and of the reaction of **2** with phosphines to yield phosphine oxides. While the latter transformation is well-precedented and not thermodynamically challenging, it lends itself readily to mechanistic analysis that can provide much needed fundamental information on the reaction pathways traversed by discrete (peroxo)diiron(III,III) species.

Results

Oxygenation Reactions. Dichloromethane or toluene solutions of the structurally defined paddlewheel complexes **1** that differ significantly only with respect to the nature of their terminal ligands (pyridine, 1-methylimidazole, or THF) react rapidly with O_2 even at low temperature (<200 K). If scrupulously purified solvent is used, a deep red-brown intermediate **2** forms with a UV−vis absorption feature at ~500−550 nm ($\epsilon \sim 1000-1200$ M^{-1} cm^{-1}, Figure 1) that decays upon warming. If the solvent is not purified suf-

(7) Newcomb, M.; Aebisher, D.; Shen, R.; Chandrasena, R. E. P.; Hollenberg, P. F.; Coon, M. J. *J. Am. Chem. Soc.* **2003**, *125*, 6064−6065.
(8) Que, L., Jr. *J. Chem. Soc., Dalton Trans.* **1997**, 3933−3940.
(9) Du Bois, J.; Mizoguchi, T. J.; Lippard, S. J. *Coord. Chem. Rev.* **2000**, *200−202*, 443−485.
(10) Que, L., Jr.; Tolman, W. B. *Angew. Chem., Int. Ed.* **2002**, *41*, 1114−1137.
(11) Girerd, J.-J.; Banse, F.; Simaan, A. J. *Struct. Bonding* **2000**, *97*, 145−177.
(12) Ookubo, T.; Sugimoto, H.; Nagayama, T.; Masuda, H.; Sata, T.; Tanaka, K.; Maeda, Y.; Okawa, H.; Hayashi, Y.; Uehara, A.; Suzuki, M. *J. Am. Chem. Soc.* **1996**, *118*, 701−702.
(13) Dong, Y.; Yan, S.; Young, V. G., Jr.; Que, L., Jr. *Angew. Chem., Int. Ed. Engl.* **1996**, *35*, 618−620.
(14) Kim, K.; Lippard, S. J. *J. Am. Chem. Soc.* **1996**, *118*, 4914−4915.
(15) Dong, Y.; Zang, Y.; Shu, L.; Wilkinson, E. C.; Que, L., Jr. *J. Am. Chem. Soc.* **1997**, *119*, 12683−12684.
(16) Feig, A. L.; Becker, M.; Schindler, S.; van Eldik, R.; Lippard, S. J. *Inorg. Chem.* **1996**, *35*, 2590−2601. Correction: Feig, A. L.; Becker, M.; Schindler, S.; van Eldik, R.; Lippard, S. J. *Inorg. Chem.* **2003**, *42*, 3704.
(17) Herold, S.; Lippard, S. J. *J. Am. Chem. Soc.* **1997**, *119*, 145−156.
(18) Feig, A. L.; Masschelein, Z.; Bakac, A.; Lippard, S. J. *J. Am. Chem. Soc.* **1997**, *119*, 334−342.
(19) LeCloux, D. D.; Barrios, A. M.; Mizoguchi, T. J.; Lippard, S. J. *J. Am. Chem. Soc.* **1998**, *120*, 9001−9014.
(20) Sugimoto, H.; Nagayama, T.; Maruyama, S.; Fujinami, S.; Yasuda, Y.; Suzuki, M.; Uehara, A. *Bull. Chem. Soc. Jpn.* **1998**, *71*, 2267−2279.
(21) LeCloux, D. D.; Barrios, A. M.; Lippard, S. J. *Biorg. Med. Chem.* **1999**, *7*, 763−772.
(22) Kryatov, S. V.; Rybak-Akimova, E. V.; MacMurdo, V. L.; Que, L., Jr. *Inorg. Chem.* **2001**, *40*, 2220−2228.
(23) Costas, M.; Cady, C. W.; Kryatov, S. V.; Ray, M.; Ryan, M. J.; Rybak-Akimova, E. V.; Que, L., Jr. *Inorg. Chem.* **2003**, *42*, 7519−7530.
(24) Yoon, S.; Lippard, S. J. *Inorg. Chem.* **2003**, *42*, 8606−8608.
(25) Que, L., Jr.; Tolman, W. B. *J. Chem. Soc., Dalton Trans.* **2002**, 653−660.
(26) Chavez, F. A.; Ho, R. Y. N.; Pink, M.; Young, V. G., Jr.; Kryatov, S. V.; Rybak-Akimova, E. V.; Andres, H. P.; Münck, E.; Que, L., Jr.; Tolman, W. B. *Angew. Chem., Int. Ed.* **2002**, *41*, 149−152.
(27) Brunold, T. C.; Tamura, N.; Kitajima, N.; Moro-oka, Y.; Solomon, E. I. *J. Am. Chem. Soc.* **1998**, *120*, 5674−5690.
(28) Neese, F.; Solomon, E. I. *J. Am. Chem. Soc.* **1998**, *120*, 12829−12848.

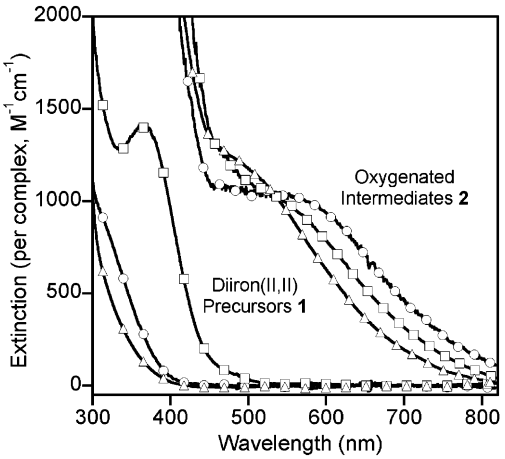

Figure 1. Electronic absorption spectra of the diiron(II,II) precursors **1-Py** (□), **1-MeIm** (Δ), **1-THF** (○), and their respective dioxygen adducts **2-Py** (□), **2-MeIm** (Δ), and **2-THF** (○) generated in batch experiments, in CH_2Cl_2 at 193 K.

ficiently, or trace water is added purposefully, the red-brown color fails to develop, and instead, a yellow chromophore forms that does not change upon warming. This species has not been characterized, although we suspect that it is some type of an iron(III)-carboxylate complex. Importantly in the context of the kinetic studies reported herein, the intense UV−vis absorbance feature at ∼550 nm is convenient for the observation of the formation and decay of **2**, particularly because other participating species (diferrous precursors, decomposition products, and products of oxygenation in contaminated solvent) do not absorb significantly at this wavelength. In addition, the UV−vis spectra of **2-py**, **2-MeIm**, and **2-THF** are distinct (Figure 1), indicating that the different capping pyridine, 1-methylimidazole, and THF ligands remain bound to the iron centers in the oxygenation process.

Stopped-flow studies of the oxygenation of compounds **1** in rigorously dried CH_2Cl_2 were performed between 193 and 293 K using UV−vis spectroscopic monitoring. The resulting peroxo intermediates **2** are stable for hours at 193 K, and in the temperature range 193−223 K, their decay is very slow on the stopped-flow time scale. Above 223 K, both formation and decomposition (see below) of the peroxo intermediates could be studied by stopped-flow spectrophotometry. The oxygenation kinetics for **1-py**, **1-MeIm**, and **1-THF** were found to be similar. Under conditions of excess dioxygen, the formation of the peroxo intermediates **2** follows a pseudo-first-order rate law. The pseudo-first-order rate constants are independent of the starting concentrations of the diiron(II,-II) complexes and display linear dependencies on the concentration of dioxygen (in excess, Figure 2). When equimolar concentrations of a diiron(II,II) complex and O_2 are used, overall second-order kinetics are observed (Figure 3). Nearly identical values for the second-order rate constants (k) were obtained under the pseudo-first- and second-order concentration conditions (Table S1). Taken together, the data show that the oxygenation reactions follow the rate law shown in eq 1. It should be noted that a 1:1 stoichiometry for the reactions is confirmed by the excellent second-order fits obtained over three or more half-lives when a 1:1 ratio

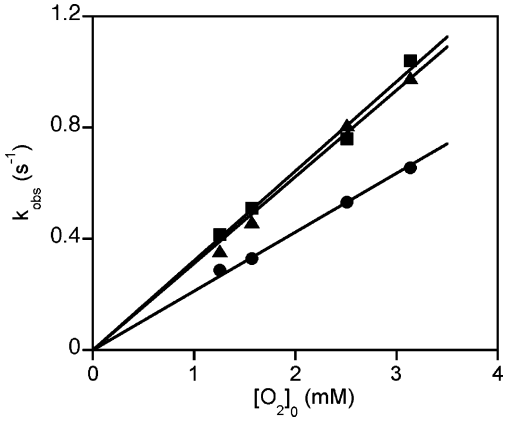

Figure 2. Plot of pseudo-first-order rate constants for the oxygenations of **1-Py** (●), **1-MeIm** (▲), and **1-THF** (■) as a function of the concentration of dioxygen. Conditions: $T = 233$ K, $[\mathbf{1}]_0 = 3 \times 10^{-4}$ M in CH_2Cl_2.

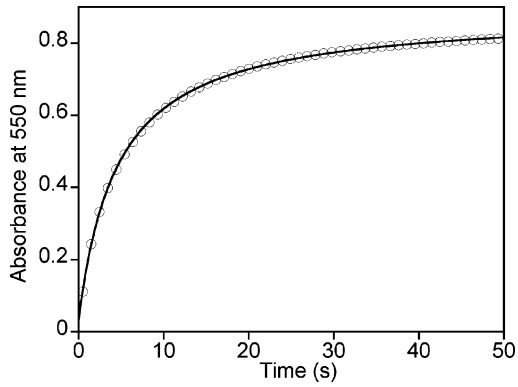

Figure 3. A representative oxygenation reaction kinetic trace obtained by stopped-flow spectrophotometry (550 nm), for the conversion of **1-Py** to **2-Py** with every 10th data point shown and a superimposed second-order kinetic fit. Conditions: $T = 203$ K, $[\mathbf{1\text{-}Py}]_0 = [O_2]_0 = 1.63$ mM in CH_2Cl_2.

of diiron(II,II) precursor and dioxygen was used. Under a different stoichiometry, one of the reagents would be exhausted before the other, and eq 1 would no longer fit the experimental kinetic data in satisfactory fashion.

$$\frac{d[\mathbf{2}]}{dt} = k[\mathbf{1}][O_2] \qquad (1)$$

Eyring plots of the second-order rate constants were linear for all three reactions (Figure 4a) and yielded the activation parameters listed in Table 1. An isokinetic temperature T for the series is suggested by the common intersection point of the linear fits to the Eyring plots at 216 ± 4 K.[29] In addition, an enthalpy−entropy compensation effect appears evident from the plot of $\Delta H^{\ddagger}$ versus $\Delta S^{\ddagger}$ values (Figure 4b), although we note caveats associated with this type of analysis.[30] Still, the slope of the linear fit to these data yields $T = 215 \pm 4$ K, identical within experimental error to the Eyring plot intersection point value. The apparent observation of both isokinetic and enthalpy−entropy compensation

(29) (a) Schmid, R.; Sapunov, V. N. *Nonformal kinetics*; Verlag Chemie: Weinheim, 1982. (b) Linert, W.; Jameson, R. F. *Chem. Soc. Rev.* **1989**, *18*, 477−505. (c) Linert, W. *Chem. Soc. Rev.* **1994**, *23*, 429. (d) Liu, L.; Guo, Q.-X. *Chem. Rev.* **2001**, *101*, 673−695.

(30) (a) McBane, G. C. *J. Chem. Educ.* **1998**, *75*, 919. (b) Exner, O. *Prog. Phys. Org. Chem.* **1973**, *10*, 411−482.

Table 1. Activation Parameters for Reactions of Diiron(II,II) Complexes with O_2[a]

complex	solvent	$\Delta H^{\ddagger}$ (kJ mol^{-1})	$\Delta S^{\ddagger}$ (J K^{-1} mol^{-1})	ref
1-Py	CH_2Cl_2	4.7 ± 0.5	−178 ± 10	*b*
1-MeIm	CH_2Cl_2	10.1 ± 1.0	−153 ± 10	*b*
1-THF	CH_2Cl_2	14.0 ± 1.0	−135 ± 10	*b*
$[(HPTP)Fe_2(O_2CPh)]^{2+}$	EtCN	16.5 ± 0.4	−114 ± 2	16
$[(HPTP)Fe_2(O_2CPh)]^{2+}$	$CH_3CN/DMSO$[c]	8.0 ± 1.0	−143 ± 10	23
$[(HPTP)Fe_2(O_2CPh)_2]^{+}$	CH_3CN/CH_2Cl_2[d]	16.3 ± 1.0	−120 ± 10	23
$[(EtHPTB)Fe_2(O_2CPh)]^{2+}$	EtCN	15.4 ± 0.6	−121 ± 3	16
$[(HPTMP)Fe_2(O_2CPh)]^{2+}$	EtCN	42.2 ± 1.6	−63 ± 6	16
$[(PXDK)Fe_2(MeIm)_2(O_2CtBu)_2]$	THF	∼11	∼ −150	17
$[(6\text{-}Me_3TPA)_2Fe_2(OH)_2]^{2+}$	CH_2Cl_2	17 ± 2	−175 ± 20	22

[a] Drawings of the ligands abbreviated as HPTP, EtHPTB, PXDK, and 6-Me_3TPA are shown here; MeIm = 1-methylimidazole. [b] This work. [c] 9:1 v/v. [d] 1:1 v/v.

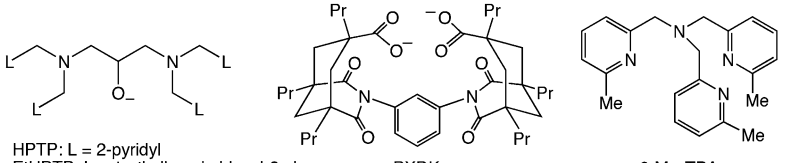

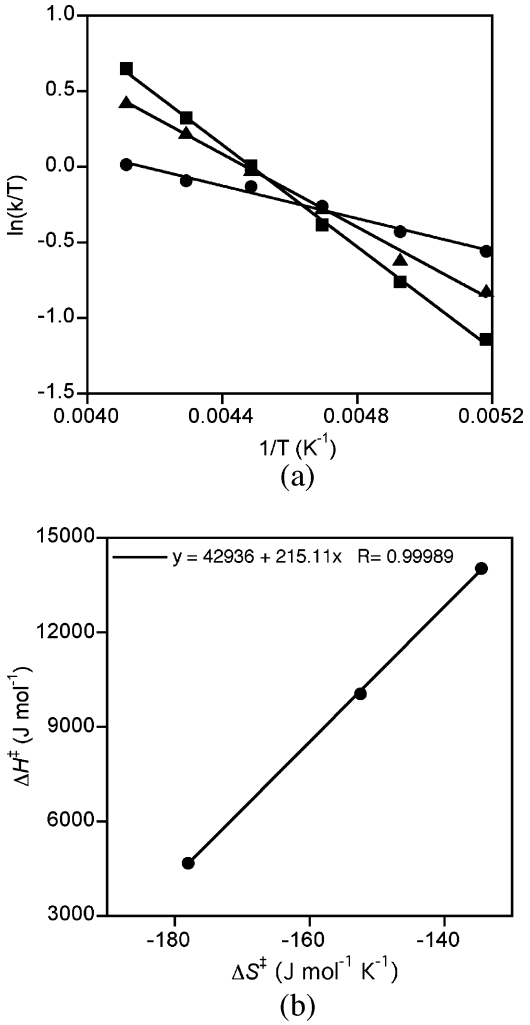

Figure 4. (a) Eyring plots for the second-order rate constants for the oxygenation of **1-Py** (●), **1-MeIm** (▲), and **1-THF** (■). (b) Correlation between the enthalpies and entropies of activation for the oxygenations of the complexes **1**.

effects is consistent with a common mechanism for the oxygenation reaction across the series of complexes **1**. Interestingly, the isokinetic temperature falls within the range of temperatures actually used in the kinetic experiments; this is a rare observation in chemical kinetics that is typically precluded by experimental or mechanistic limitations.[29]

Table 2. Activation Parameters for Reactions of (peroxo)Diiron(III,III) Complexes

reaction	$\Delta H^{\ddagger}$ (kJ mol^{-1})	$\Delta S^{\ddagger}$ (J K^{-1} mol^{-1})
2-Py decay	14.2 ± 1.0	−44 ± 10
2-MeIm decay	11.9 ± 1.0	−73 ± 10
2-THF decay	11.6 ± 1.0	−72 ± 10
2-THF + PPh_3[a]	52 ± 2	+15 ± 10
2-THF + Py[a]	52 ± 2	+15 ± 10

[a] Values correspond to the saturation rate constants, k_1, in eqs 3 and 4.

Decomposition of Peroxo Species 2 in the Absence of Substrate. As a prerequisite for studies of the reactions of the peroxo complexes **2** with added substrates, we examined the decomposition of the complexes in the absence of added reagents. Although stable for extended periods at temperatures below 233 K, above this temperature formation of the adducts **2** was followed by decomposition at rates amenable to assay by stopped-flow spectrophotometry. The most stable in the series is **2-Py**, which exhibited first-order kinetics for decomposition with rate constants (k') that were independent of [**2-Py**]$_0$ (0.3−1.5 mM) and were unperturbed by the presence of excess O_2. Activation parameters were determined from a linear Eyring plot between 243 and 293 K (Figure S1, Table 2), with a half-life $t_{1/2}$ = 180 s determined at 243 K that extrapolated to $t_{1/2}$ = 5 days at 193 K. The adducts **2-MeIm** and **2-THF** were much less stable and followed single-exponential kinetics only under conditions when excess O_2 was avoided. Linear Eyring plots were obtained under these conditions which provided activation parameters distinct from those observed for **2-Py** (Table 2). At 243 K, the $t_{1/2}$ values for **2-MeIm** and **2-THF** were 50 and 23 s, respectively, which extrapolated to 10 and 4 h at 193 K. In the presence of excess dioxygen, the decomposition of these two intermediates accelerated by 2−5 times, became poorly reproducible, and could no longer be fit in satisfactory fashion to a single-exponential kinetic equation. These data

suggest that the mechanism of decomposition of **2-MeIm** and **2-THF** changes in the presence of excess O_2.

Reaction of Peroxo Species 2 with PPh_3. (a) Batch Experiments. The trend in decomposition rates (**2-THF** > **2-MeIm** > **2-Py**) also is paralleled by the relative reactivity of the series of peroxo complexes with PPh_3. Thus, the spectroscopic features of **2-THF** (purged of free O_2) bleached rapidly (within seconds) upon addition of 2 equiv of PPh_3 at 193 K, whereas no change occurred over 10−15 min upon similar treatment of **2-MeIm** or **2-Py**. Addition of 2 equiv of pyridine to **2-THF** prior to injection of PPh_3 at 193 K caused no color change discernible by eye and inhibited bleaching by the added phosphine. These data suggest that the THF ligands in **2-THF** are replaced by pyridines to yield **2-Py**, which is inert toward PPh_3 at 193 K; kinetics data presented below corroborate this hypothesis. The rapid reaction of **2-THF** with PPh_3 (2 equiv) at 193 K provided $OPPh_3$ in 82% yield (based on **2-THF**) upon quenching of the product solution with aqueous NH_3, warming, and extraction of the organic soluble portion (with a total recovery of $OPPh_3$ and excess PPh_3 of 80%). In a control experiment, less than 4% yield of $OPPh_3$ (based on **2-THF**) was isolated when the protocol was repeated, but without any diiron reagent. Finally, when the experiment was repeated using $^{18}O_2$, analysis of the product $OPPh_3$ by mass spectrometry showed ∼90% ^{18}O incorporation, thus showing that the O atom transferred to PPh_3 derived from the peroxide ligand in **2-THF**.

(b) Stopped-Flow Kinetics. Double-mixing stopped-flow experiments were performed to gain mechanistic insight into the reactivity of complexes **2** with PPh_3. In the first mixing step, CH_2Cl_2 solutions of **1** and O_2 were combined at 193 K and incubated for sufficient time (∼50−100 s) to ensure complete formation of the respective peroxo complex, **2**. Then, the solution of **2** was mixed at 193 K with a CH_2Cl_2 solution of substrate (PPh_3, or other reagents, as described below), and changes in optical absorbance at 550 nm were monitored. Experiments with **2-Py** and **2-MeIm** confirmed that they do not lose optical absorbance to any significant extent within 3−5 min upon mixing with PPh_3 at 193 K. Moreover, the rates of decomposition of **2-Py** and **2-Im** at 243 K were not altered signficantly in the presence of 10 equiv of PPh_3.

In contrast, mixing solutions of **2-THF** and PPh_3 (equivalent amount or an excess) in the stopped-flow instrument led to a fast reaction, complete within seconds at 193 K. Under conditions of a large excess of PPh_3, decay of the optical absorbance associated with **2-THF** displayed pseudo-first-order kinetics (Figure 5, eq 2), with temperature-dependent pseudo-first-order rate constants (k_{obs}) that yielded a linear Eyring plot (Figure 6, circles) and the activation parameters listed in Table 2. Importantly, assessment of the dependence of k_{obs} on $[PPh_3]_0$ revealed saturation behavior (Figure 7, ●) that is consistent with a mechanism involving binding of substrate to **2-THF**. Moreover, added THF inhibits the reaction of **2-THF** with PPh_3, such that k_{obs} decreases with increasing $[THF]_0$ according to the saturation curve shown in Figure 7 (◆, under conditions of constant excess

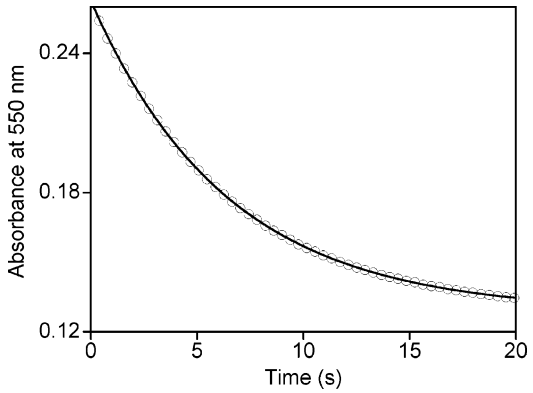

Figure 5. A representative kinetic trace for the reaction of **2-THF** with excess PPh_3 obtained by double-mixing stopped-flow spectrophotometry (550 nm), with every 10th data point shown and a superimposed pseudo-first-order kinetic fit. Conditions: $T = 193$ K, $[\mathbf{2\text{-}THF}]_0 = 0.3$ mM, $[PPh_3]_0 = 9.5$ mM, in CH_2Cl_2.

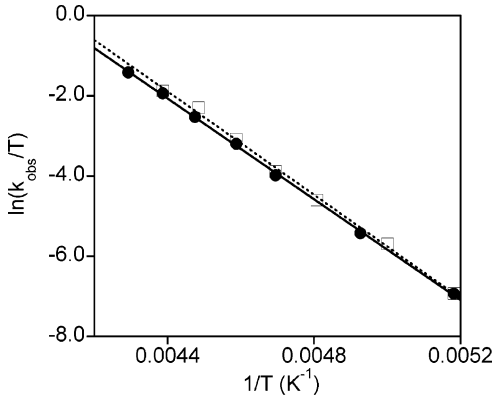

Figure 6. Eyring plots of the pseudo-first-order rate constants (k_{obs}) for the reaction of **2-THF** with excess PPh_3 (●) and excess Py (□) obtained by double-mixing stopped-flow spectrophotometry. Conditions: $[\mathbf{2\text{-}THF}]_0 = 0.3$ mM, $[PPh_3]_0$ or $[Py]_0 = 9.5$ mM, in CH_2Cl_2.

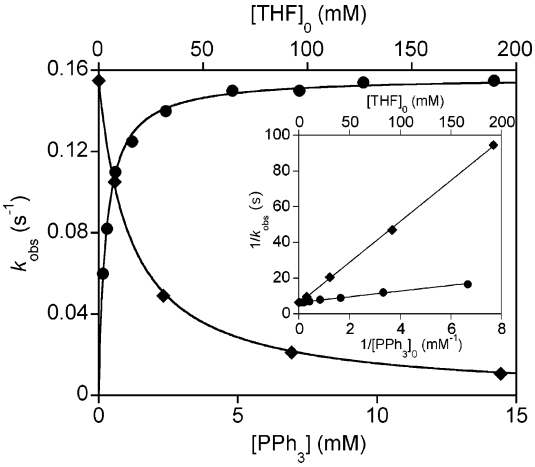

Figure 7. Plot of the pseudo-first-order rate constant k_{obs} for the reaction of **2-THF** with PPh_3 as a function of $[PPh_3]_0$ (●) and added $[THF]_0$ (◆), at constant $[PPh_3]_0 = 7.5$ mM. The lines are fits to eq 3. The inset shows the same data plotted as $1/k_{obs}$ versus $1/[PPh_3]_0$ (●) and added $[THF]_0$ (◆), at constant $[PPh_3]_0 = 7.5$ mM, with linear fits. Conditions: $T = 193$ K, $[\mathbf{2\text{-}THF}]_0 = 0.3$ mM.

$[PPh_3]_0$). The inset to Figure 7 shows the data replotted as straight lines in the coordinates $1/k_{obs}$ versus $1/[PPh_3]_0$ (●) and $[THF]_0$ (◆). Taken together, the kinetic data indicate that substitution of coordinated THF by PPh_3 occurs prior to substrate oxidation by **2-THF**. The dependence of k_{obs} on

Table 3. Saturation Rate Constants for the Reactions of **2-THF** with Phosphines and N-Donor Ligands[a]

reagent	k_1 (s^{-1})
$P(p\text{-}C_6H_4Cl)_3$	0.18 ± 0.02
$P(p\text{-}C_6H_4F)_3$	0.18 ± 0.02
PPh_3	0.17 ± 0.03
$P(p\text{-}C_6H_4Me)_3$	0.18 ± 0.02
$P(p\text{-}C_6H_4OMe)_3$	0.06 ± 0.01
Py	0.19 ± 0.02
MeIm	0.19 ± 0.02

[a] Conditions: CH_2Cl_2, 193 K, [**2-THF**] = 0.2−0.3 mM, [reagent] = 5−10 mM unless noted otherwise.

$[PPh_3]_0$ and $[THF]_0$ may be described by eq 3, where k_1 is the maximum possible rate constant under conditions of saturating $[PPh_3]_0$ (i.e., the pseudo-first-order rate constant when a large excess of PPh_3 is used), and the ratio k_2/k_{-1} represents the relative affinities or reactivities of PPh_3 and THF to an iron center in **2-THF** (see Discussion section). Fitting of the data to eq 3 yielded the parameters $k_1 = 0.17 \pm 0.03\ s^{-1}$ and $k_2/k_{-1} = 1.7 \pm 0.2$ at 193 K.

$$\frac{d[\mathbf{2\text{-}THF}]}{dt} = -k_{obs}[\mathbf{2\text{-}THF}] \quad (2)$$

$$k_{obs} = \frac{k_1 k_2[PPh_3]}{k_{-1}[THF] + k_2[PPh_3]} \quad (3)$$

To shed further light on the oxidation mechanism, the kinetics of the reactions of a series of derivatives of PPh_3 with electron-withdrawing (Cl, F) and -donating (Me, OMe) *para* phenyl substituents were examined. Typically, the reactivity of the triaryl phosphines with oxidizers or electrophiles increases in the following order: $P(p\text{-}C_6H_4Cl)_3 < P(p\text{-}C_6H_4F)_3 < PPh_3 < P(p\text{-}C_6H_4Me)_3 < P(p\text{-}C_6H_4OMe)_3$.[31] Similar to the reaction with the parent reagent PPh_3, fast disappearance of intermediate **2-THF** in CH_2Cl_2 at 193 K occurred upon addition of an excess amount of each of the substituted phosphines. Stopped-flow kinetic data showed that the reactions were first-order in **2-THF** and zero-order in the phosphine used in excess. Importantly, the first-order rate constants under saturating phosphine concentrations (k_1, Table 3) were essentially the same for all of the phosphines ($P(p\text{-}C_6H_4Cl)_3$, $P(p\text{-}C_6H_4F)_3$, PPh_3, and $P(p\text{-}C_6H_4Me)_3$), except $P(p\text{-}C_6H_4OMe)_3$, for which k_1 was significantly smaller. The identical reactivity of the former four phosphines (*para* substituents Cl, F, H, and Me) indicates that neither coordination to the metal nor a redox transformation is the rate-limiting step in the overall reaction. Instead, the data suggest that the rate of the overall transformation is limited by dissociation of the THF ligand from **2-THF**. The anomalous behavior of $P(p\text{-}C_6H_4OMe)_3$ may be rationalized by invoking complications due to binding of its ether subunits to the metal, in competition with THF and/or the phosphorus atom. In such a scenario, the O-bound $P(p\text{-}C_6H_4OMe)_3$ would have to dissociate and recoordinate via the P-atom in order for the phosphine reaction to ensue, the net result being an overall inhibition of the reaction rate.

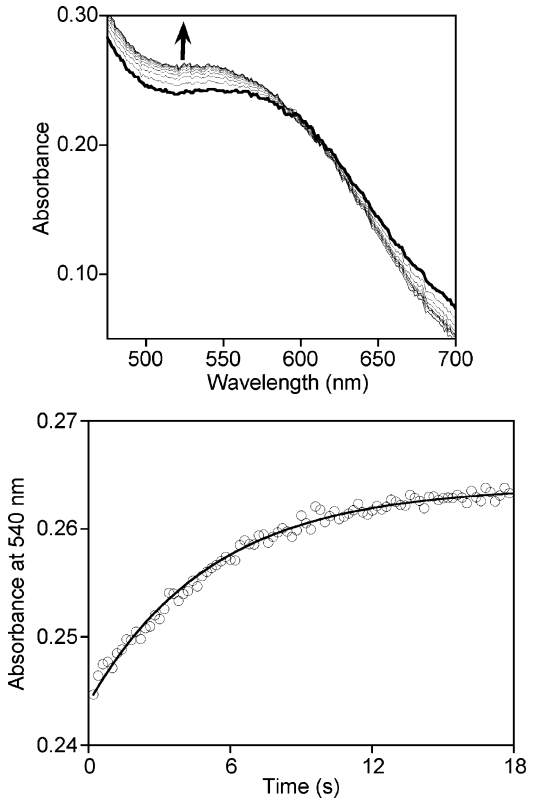

Figure 8. Top: UV−vis spectra as a function of time for the reaction of **2-THF** with pyridine. Bottom: Representative kinetic trace at 540 nm for the reaction of **2-THF** with pyridine, with a pseudo-first-order fit. Conditions: $T = 193$ K, $[\mathbf{2\text{-}THF}]_0 = 0.25$ mM; $[Py]_0 = 5$ mM.

In order to test the hypothesis that THF dissociation is rate-limiting in the reactions of **2-THF** with phosphines, we examined alternate ligand substitution reactions of this complex that would not be complicated by a subsequent redox transformation. Because we had observed that **2-Py** and **2-MeIm** were much less reactive with PPh_3 than **2-THF**, which reacted according to the rate law in eq 3, we reasoned (a) that Py and MeIm coordinated more strongly than THF to the iron centers in **2**, and (b) that the conversions of **2-THF** to **2-Py** or **2-MeIm** through simple ligand substitution reactions would be feasible. Thus, we examined the reactions of **2-THF** with Py and MeIm by double-mixing stopped-flow spectrophotometry. As expected from the data shown in Figure 1, relatively small spectral changes were observed upon mixing solutions of **2-THF** and Py or MeIm in CH_2Cl_2 at 193 K (cf., results with added Py in Figure 8). Nevertheless, the changes were consistent with retention of the (peroxo)diiron(III,III) core as substitution proceeded and were of sufficient magnitude to enable important kinetic information to be extracted. Thus, the reactions between **2-THF** and Py or MeIm (used in excess) were first-order in **2-THF** and showed saturation behavior as the N-ligand concentration was varied, as illustrated by the linear plot of $1/k_{obs}$ versus $1/[Py]_0$ in Figure 9 (●). The values of the saturation rate constants (k_1) were nearly the same for the two N-ligands ($0.19 \pm 0.02\ s^{-1}$), and were essentially the same as the corresponding values observed for the reactions

(31) (a) Huang, R.; Espenson, J. H. *J. Mol. Catal. A: Chem.* **2001**, *168*, 39−46. (b) Wang, Y.; Espenson, J. H. *Inorg. Chem.* **2002**, *41*, 2266−2274. (c) Dixon, J.; Espenson, J. H. *Inorg. Chem.* **2002**, *41*, 4727−4731.

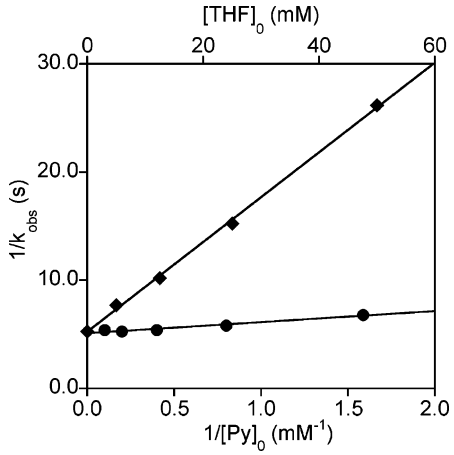

Figure 9. Plot of the pseudo-first-order rate constant k_{obs} for the reaction of **2-THF** with pyridine plotted as $1/k_{obs}$ versus $1/[Py]_0$ (●) and added $[THF]_0$ (◆, at constant $[Py]_0 = 5.0$ mM), with linear fits. Conditions: $T =$ 193 K, $[\mathbf{2\text{-}THF}]_0 = 0.3$ mM.

of **2-THF** with phosphines (0.17 ± 0.03 s^{-1}). Most significantly, the rate constants k_1 for the reactions of **2-THF** with excess Py and PPh_3 were found to be closely similar in the temperature range 193−233 K, yielding activation parameters for the two different reactions that were identical within experimental error (Figure 6, Table 2). In addition to exhibiting saturation behavior as the N-ligand concentration was increased, the reaction between **2-THF** and Py at 193 K is retarded by added THF, such that a plot of $1/k_{obs}$ versus $[THF]_0$ is linear (Figure 9, ◆). Thus, the experimental rate equation for the reaction of **2-THF** with Py (eq 4) is of the same form as that for its reaction with PPh_3 (eq 3), with fits that yield closely similar values for the parameters k_1 (PPh_3, 0.17 ± 0.03 s^{-1}; Py, 0.19 ± 0.02 s^{-1}) and k_2/k_{-1} (PPh_3, 1.7 ± 0.2; Py, 2.5 ± 0.3). Taken together, the kinetics data for the reactions of **2-THF** with N-donor ligands show that (a) they are mechanistically analogous to the reactions of **2-THF** with phosphines and (b) the rate of ligand substitution in **2-THF** is controlled by the dissociation of THF.

$$k_{obs} = \frac{k_1 k_2 [Py]}{k_{-1}[THF] + k_2[Py]} \qquad (4)$$

Discussion

Oxygenation Reactions. The kinetic data for the reactions of complexes **1** with O_2 in CH_2Cl_2 are consistent with a common mechanism for the series of diiron(II,II) precursors involving an associative, bimolecular rate-determining step. This conclusion is supported by the overall second-order rate law (eq 1), the small enthalpies and negative (unfavorable) entropies of activation (Table 1), and the observation of an isokinetic effect and an activation enthalpy/entropy correlation (Figure 4). The finding of similar kinetic parameters for the complexes containing both strong (Py, MeIm) and poor (THF) donors suggests that electronic effects are minor, in agreement with reports on mononuclear O_2 carriers where O_2 dissociation rates depend strongly on electronic effects, but O_2 binding rates do not.[32,33] Dissociation of THF, Py, or MeIm ligands upon O_2 binding does not appear to occur on the basis of the general similarity yet subtle specific differences in the UV−vis spectra of the adducts **2** (Figure 1), as well as the finding that **2-THF** may be converted to **2-Py** or **2-MeIm** by addition of Py or MeIm, respectively. Comparison of the kinetic results to those reported for other diiron(II,II) systems that yield (peroxo)diiron(III,III) complexes (cf. activation parameters in Table 1) reveals general similarities, in particular a common associative pathway that is entropically controlled.[16,17,22,23] The $\Delta H^{\ddagger}$ value for oxygenation of **1-Py** is notably less than the other reported systems, and this low value and the other modest ones for **1-MeIm** and **1-THF** are consistent with little if any contribution of a ligand substitution process to the O_2 binding event. In other words, the data support direct addition of O_2 to the 5-coordinate iron(II) centers, which as a result is a quite rapid process, as seen for other mononuclear and dinuclear systems that feature coordinatively unsaturated or labile sites.[16,23,34] Accordingly, carboxylate shifts[35] that are implicated by the structural postulates for **2** must be fast relative to the rate-controlling bimolecular oxygenation.

Decomposition of Peroxo Species 2 in the Absence of Substrate. The adducts **2** prepared in solution at low temperature (e.g., 193 K) are thermally unstable and decompose upon warming. We have not isolated the final product(s), but we assume that iron(III) carboxylate complexes are formed. The decomposition kinetics were examined primarily in order to provide baseline information for comparison to data acquired on reactions of **2** with added potential substrates. The autodecay of all three complexes follows first-order kinetics (for **2-MeIm** and **2-THF**, only in the absence of excess O_2), with relatively low activation enthalpies (11.6−14.2 kJ mol^{-1}) and negative activation entropies (−73 to −44 J mol^{-1} K^{-1}). The stabilities of the adducts differ significantly and decrease in the following order ($t_{1/2}$ values at 193 K listed in parentheses): **2-Py** (5 days) > **2-MeIm** (10 h) > **2-THF** (4 h). Although **2-THF** is relatively unstable and shows correspondingly greater reactivity with substrates, its self-decay rate is sufficiently slow to obviate any possible complications in kinetic analysis of its intermolecular reactions with exogenous reagents.

Only a few studies of the kinetics of self-decomposition of (peroxo)iron complexes have been reported.[18,23,36] A peroxo-bridged iron(III) porphyrin dimer was found to decompose via a first-order process with $\Delta H^{\ddagger} = 14.5$ kJ mol^{-1} and $\Delta S^{\ddagger} = -63$ J mol^{-1} K^{-1}, and a mechanism was proposed that involved rate-determining O−O bond homolysis.[36] Bimolecular kinetics were observed for the decomposition of putative (peroxo)diiron species resulting from the oxygenation of several nonheme diiron(II,II) complexes of

(32) Wilkins, R. G. In *Oxygen Complexes and Oxygen Activation by Transition Metals*; Martell, A. E., Sawyer, D. T., Eds.; Plenum Press: New York, 1987; pp 49−60.
(33) Rybak-Akimova, E. V.; Marek, K.; Masarwa, M.; Busch, D. H. *Inorg. Chim. Acta* **1998**, *270*, 151−161.
(34) Warburton, P. R.; Busch, D. H. In *Perspectives on Bioinorganic Chemistry*; JAI Press: London, 1993; Vol. 2, pp 1−79.
(35) Rardin, R. L.; Tolman, W. B.; Lippard, S. J. *New J. Chem.* **1991**, *15*, 417−430.
(36) Chin, D.-H.; La Mar, G. N.; Balch, A. L. *J. Am. Chem. Soc.* **1980**, *102*, 4344−4350.

Scheme 2

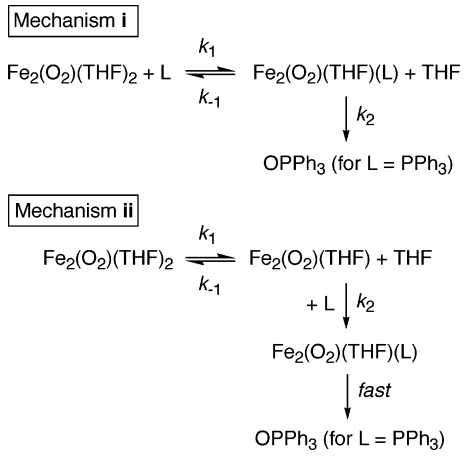

dinucleating ligands, and the intermediacy of (peroxo)tetra-iron complexes was invoked.[18] In a more recent study of these diiron systems, bimolecular pathways were suppressed by binding of additional O-donor ligands (e.g., DMSO or carboxylate), resulting in enhanced stability[13] and unimolecular decay paths for the 6-coordinate (peroxo)diiron(III,-III) complexes.[23] We speculate that, in the case of compounds **2**, a bimolecular decomposition mechanism(s) is inhibited by the steric hindrance provided by the dixylyl-carboxylate ligands. The specific basis for the first-order decay kinetics is not clear, since assessment of the detailed molecular pathway for the decomposition of **2** requires more experimental data and is beyond the scope of the present study.

Reactivity of Peroxo Species 2 with Added Substrates. The least stable intermediate, **2-THF**, was also found to be the most reactive, and it oxidized PPh_3 at low temperature (193 K)[37] at a rate much faster than self-decomposition (by a factor of 5000 at 233 K). The peroxo complexes **2-Py** and **2-MeIm** were much less reactive, and their spectroscopic features bleached in the presence of PPh_3 at rates similar to or limited by self-decay. Retardation of the reaction of **2-THF** with PPh_3 by added THF strongly suggests that substitution of a THF ligand in **2-THF** by PPh_3 represents the initial stage of the reaction. On the basis of the experimental rate law (eqs 2 and 3), two possible mechanisms may be envisaged (Scheme 2). In pathway i, a rapid ligand substitution pre-equilibrium is followed by rate-determining substrate oxidation within the coordination sphere of the (peroxo)diiron(III,III) complex. The second route (ii) involves rate-limiting dissociation of a THF ligand followed by coordination of PPh_3 and rapid inner-sphere substrate oxidation. Both mechanisms yield rate expressions consistent with the experimentally determined rate law (eqs 2 and 3).

Further analysis, however, lends specific preferential support to mechanism ii. The observation of identical saturation rate constants for the series of substituted phosphines (Table 3) is inconsistent with pathway i and favors mechanism ii. The anomalous reactivity of $P(p\text{-}C_6H_4OMe)_3$ with **2-THF** may also be rationalized by assuming that dissociative ligand substitution is the rate-limiting step (vide supra). Most importantly, the finding that the THF ligand in **2-THF** was substituted by Py and MeIm at the same rate as the reaction of **2-THF** with phosphine is strong evidence that all of these reactions are controlled kinetically by the same step, the substitution of a THF ligand on an iron(III) center in **2-THF**. The insensitivity of the reaction rate to the nature of the incoming ligand suggests that the ligand substitution proceeds by a dissociative mechanism. The relatively large enthalpy of activation and positive entropy of activation (Table 2) provide further support for a dissociative pathway. Such pathways are common for iron(III) complexes and proceed at high rates ($k = 10^4-10^7$ s^{-1} at 298 K),[38-44] but associative mechanisms also have been observed, albeit at slower rates ($k = 10^2-10^3$ s^{-1} at 298 K).[38,45] Extrapolation of the saturation rate constants for reaction of **2-THF** with PPh_3 or Py obtained at low temperature (193−233 K) to 298 K gives $k = 3 \times 10^4$ s^{-1}, which is within the range typical for dissociative substitution mechanisms. Consistent with this view, the sluggish reactivity of **2-Py** and **2-MeIm** with PPh_3 may be rationalized by slower rates of dissociation of Py or MeIm ligands compared to the more labile THF ligand in **2-THF**.

The existence of a short-lived (peroxo)diiron(III)−phosphine adduct is implied by mechanism ii (Scheme 2). There is no evidence that such an intermediate with either reducing (phosphine) or oxidizing (peroxide) ligands accumulates during the reactions of **2-THF**, suggesting that intramolecular redox (i.e., O-atom transfer from coordinated peroxide to bound phosphine) is rapid. Phosphines are more typically found to coordinate to low-valent iron, but coordination to Fe(III) is precedented,[46-48] making it reasonable to assume that the stability of an Fe(III)−PPh_3 complex would be at least comparable to that of an Fe(III)−ether or −THF species and that PPh_3 substitution for THF is feasible. On the other hand, aromatic N-donors such as Py or MeIm would be expected to bind more tightly than PPh_3 to iron(III), consistent with the decreased reactivity of **2-Py** and **2-MeIm** relative to **2-THF**.

The apparent requirement that we have found in this study for substrate coordination prior to oxidation parallels results reported for other iron and copper systems. The oxidation of PPh_3 by the (peroxo)diiron(III,III) complex supported by HPTP (see graphic with Table 1) follows saturation kinetics,[23] as do sulfide oxidations by mono- and dinuclear peroxo

(37) In preliminary experiments, we have found that **2-THF** also oxidizes PhSMe to PhS(O)Me at 243 K. Kryatov, S. V.; Rybak-Akimova, E. V.; Chavez, F. A.; Que, L., Jr.; Tolman, W. B. Unpublished results.

(38) Merbach, A. E. *Pure Appl. Chem.* **1982**, *54*, 1479−1493.
(39) Doeff, M. M.; Sweigart, D. A. *Inorg. Chem.* **1982**, *21*, 3699−3705.
(40) Zhang, Z.; Jordan, R. B. *Inorg. Chem.* **1996**, *35*, 1571−1576.
(41) Bhattacharyya, S. K.; Banerjee, R. *Polyhedron* **1997**, *16*, 849−854.
(42) Schneppensieper, T.; Zahl, A.; van Eldik, R. *Angew. Chem., Int. Ed.* **2001**, *40*, 1678−1680.
(43) Schneppensieper, T.; Seibig, S.; Zahl, A.; Tregloan, P.; van Eldik, R. *Inorg. Chem.* **2001**, *40*, 3670−3676.
(44) Ivanovic-Burmazovic, I.; Hamza, M. S. A.; van Eldik, R. *Inorg. Chem.* **2002**, *41*, 5150−5161.
(45) Watton, S. P.; Masschelein, A.; Rebek, J., Jr.; Lippard, S. J. *J. Am. Chem. Soc.* **1994**, *116*, 5196−5205.
(46) Naldini, L. *Gazz. Chim. Ital.* **1960**, *90*, 1231−1238.
(47) Walker, J. D.; Poli, R. *Inorg. Chem.* **1989**, *28*, 1793−1801.
(48) Godfrey, S. M.; Kelly, D. G.; Mackie, A. G.; MacRory, P. P.; McAuliffe, C. A.; Pritchard, R. G.; Watson, S. M. *J. Chem. Soc., Chem. Commun.* **1991**, 1447−1449.

compounds with low-spin iron(III) centers that are supported by substituted dipyridyl ligands.[49,50] Direct kinetic data also indicate that coordination of phenolates and thioethers to the metal centers in bis(μ-oxo)dicopper complexes precedes oxidation of these substrates,[51,52] and indirect support for similar precoordination of other substrates to such cores has been presented.[53,54] In other cases, a notable lack of electrophilic oxidation activity may be rationalized by the absence of a vacant or labile coordination site for substrate binding. For example, 6-coordinate (peroxo)diiron(III,III) complexes of PXDK and analogues (see drawing Table 1) were unreactive with PPh_3 and instead exhibited nucleophilic behavior at low temperature (e.g., evolved H_2O_2 upon treatment with phenols).[21] Such nucleophilic reactivity also is documented for coordinatively saturated (peroxo)iron(III)porphyrin complexes.[55] Finally, we note parenthetically a recent relevant report of the generation of $OPPh_3$ when a diiron(II,II) complex with sterically hindered 2,6-ditolylbenzoates and capping Me_3TACN ligands was oxygenated at 195 K in the presence of PPh_3.[56] Although an oxygenated intermediate appears to form at this temperature in the absence of PPh_3, control experiments were interpreted to suggest that a derived (oxo)diiron(III,III) complex is responsible for $OPPh_3$ generation.

It is not possible to discern from the available data how $OPPh_3$ evolves from the putative intermediate comprising coordinated PPh_3 and a peroxide ligand (Scheme 2) in the reaction of **2-THF**. One may envision that direct O-atom transfer from the peroxide occurs, or that PPh_3 coordination triggers peroxide O−O bond scission to yield a high valent species (e.g., with an Fe(IV)═O unit(s))[57] that is the active oxidant. A route similar to the latter has been proposed for oxidative dealkylation of a coordinated amine upon oxygenation of a diiron(II) carboxylate complex.[58]

Conclusion

Mechanistic studies using cryogenic stopped-flow kinetic methods have shown that dioxygen is bound in a direct low-barrier associative pathway by the diiron(II,II) complexes **1** supported by the sterically hindered carboxylate **A** to form (peroxo)diiron(III,III) intermediates **2**. The intermediates containing Py or MeIm do not react with added PPh_3 at low temperature and instead undergo slow decomposition. On the other hand, **2-THF** was found to perform a fast single-turnover oxygen-atom transfer from dioxygen to PPh_3 at low temperatures, which is kinetically controlled by the dissociation of a THF ligand. We propose mechanism ii (Scheme 2) for the reaction, with key supporting evidence including saturation kinetic behavior with substrate, inhibition by added THF, and identical saturation rate constants for oxidation of a set of phosphine deriviatives with variable *para* substituents as well as simple ligand substitution of THF by added Py or MeIm. Proximity of a reducing substrate to the coordinated peroxo ligand appears be a key prerequisite for reaction in the complexes examined here and in other synthetic oxidation systems where substrate coordination to the iron center is possible. In enzymes, the electrophilic reactivity of an iron(III)-bound peroxide ligand might be similarly enhanced by proximity of a substrate to the iron-peroxo active site, which might be achieved either by coordination or by noncovalent binding in a pocket or cavity shaped by the enzyme tertiary structure.

Experimental Section

Materials. The complexes **1-Py**, **1-MeIm**, and **1-THF** were prepared as described previously.[26] All manipulations with the complexes and their solutions were carried out under strictly anaerobic conditions. Dichloromethane (Fisher, >99.9%, GS/MS grade, not stabilized) was distilled from CaH_2 and additionally treated with basic alumina, which had been activated at 443−453 K under vacuum for 6 h. Dioxygen and dinitrogen (ultrahigh purity grade, Airgas Northeast) were passed through a column with drierite. Graduated mixtures of oxygen and nitrogen were prepared using Bel-Art gas flow meters. Saturated solutions of O_2 and calibrated O_2-N_2 mixtures in CH_2Cl_2 for the kinetic studies were prepared by bubbling the gas through the liquid for 10 min in a gastight syringe inside a gas bag filled with dry dinitrogen. The solubility of O_2 in CH_2Cl_2 was accepted to be as reported in the literature, 5.80 mM at 293 K.[59] $^{18}O_2$ was obtained from Icon Isotopes, Inc.

Kinetic Studies. The kinetic measurements were performed using a Hi-Tech Scientific (Salisbury, Wiltshire, U.K.) SF-43 cryogenic double-mixing stopped-flow instrument equipped with stainless steel plumbing, a 1.00 cm stainless steel mixing cell with sapphire windows, and an anaerobic gas-flushing kit. The instrument was connected to an IBM computer with IS-2 Rapid Kinetics Software by Hi-Tech Scientific. The mixing cell was maintained to ±0.1 K, and the mixing time was 2−3 ms. The anaerobic kit of the apparatus was flushed with dinitrogen before and during the experiments. All lines of the SF instrument were extensively washed with dioxygen-free, argon-saturated anhydrous solvent before charging the mixing syringes with reactant solutions. The starting concentrations of the reactants were corrected for the 1:1 mixing ratio and for the thermal contraction of the solvent as described previously.[60]

The reactions were generally monitored for three half-lives, and the raw kinetic data were treated with IS-2 Rapid Kinetics software from Hi-Tech Scientific, Spectfit/32 Global Analysis System software from Spectrum Software Associates, or Excel Solver from Microsoft. For example, eqs 5 and 6 were used in Excel to treat

(49) Duboc-Toia, C.; Menage, S.; Ho, R. Y. N.; Que, L., Jr.; Lambeaux, C.; Fontecave, M. *Inorg. Chem.* **1999**, *38*, 1261−1268.
(50) Mekmouche, Y.; Hummel, H.; Ho, R. Y. N.; Que, L., Jr.; Schunemann, V.; Thomas, F.; Trautwein, A. X.; Lebrun, C.; Gorgy, K.; Lepretre, J. C.; Collomb, M. N.; Deronzier, A.; Fontecave, M.; Menage, S. *Chem. Eur. J.* **2002**, *8*, 1196−1204.
(51) Itoh, S.; Kumei, H.; Taki, M.; Nagatomo, S.; Kitagawa, T.; Fukuzumi, S. *J. Am. Chem. Soc.* **2001**, *123*, 6708−6709.
(52) Taki, M.; Itoh, S.; Fukuzumi, S. *J. Am. Chem. Soc.* **2002**, *124*, 998−1002.
(53) Mahadevan, V.; DuBois, J. L.; Hedman, B.; Hodgson, K. O.; Stack, T. D. P. *J. Am. Chem. Soc.* **1999**, *121*, 5583−5584.
(54) Mahadevan, V.; Henson, M. J.; Solomon, E. I.; Stack, T. D. P. *J. Am. Chem. Soc.* **2000**, *122*, 10249−10250.
(55) Wertz, D. L.; Valentine, J. S. *Struct. Bonding* **2000**, *97*, 37−60.
(56) Tshuva, E. Y.; Lee, D.; Bu, W.; Lippard, S. J. *J. Am. Chem. Soc.* **2002**, *124*, 2416−2417.
(57) Rohde, J.-U.; In, H.-H.; Lim, M. H.; Brennessel, W. W.; Bukowski, M. R.; Stubna, A.; Münck, E.; Nam, W.; Que, L., Jr. *Science* **2003**, *299*, 1037−1039.
(58) Lee, D.; Lippard, S. J. *Inorg. Chem.* **2002**, *41*, 827−837.
(59) *Solubility Data Series. Vol. 7. Oxygen and Ozone*; Battion, R., Ed.; Pergamon: Oxford, U.K., 1981.
(60) Kryatov, S. V.; Rybak-Akimova, E. V.; MacMurdo, V. L.; Que, L., Jr. *Inorg. Chem.* **2001**, *40*, 2220−2228.

pseudo-first-order and second-order kinetic traces, respectively. In these equations, A_t stands for the experimentally measured optical absorbance at time t, with fit parameters A_0 (optical absorbance at time zero), A_∞ (optical absorbance at infinite time), k_1 (pseudo-first-order rate constant, s^{-1}), and k_2C (where k_2 is the second-order rate constant, $M^{-1}\ s^{-1}$, and C is the concentration of the reagents under equimolar conditions, M).

$$A_t = A_\infty - (A_\infty - A_0)\exp(-k_1 t) \tag{5}$$

$$A_t = A_\infty - \frac{(A_\infty - A_0)}{(1 + k_2 C t)} \tag{6}$$

The reactions between the diferrous complexes **1** and dioxygen were studied in CH_2Cl_2 solution in the temperature range 193−293 K. The concentrations of the reactant solutions before mixing were varied from 0.25 to 2.9 mM in diferrous complex and from 1.45 to 5.8 mM in O_2, with dioxygen used either in large excess (pseudo-first-order conditions) or in a stoichiometric amount (second-order conditions). At temperatures higher than 233 K, the formation of the dioxygen adducts (**2**) was followed by their spontaneous decomposition, but in most cases the two kinetic stages had significantly different time scales and could be treated independently. Under some temperature and concentration conditions, however, the formation and decomposition stages overlapped, in which cases the double-exponential fitting protocol in the IS-2 Rapid Kinetics or Spectfit/32 software was used to extract the rate constants. The formation and decomposition of the dioxygen adducts **2** were monitored at 550 nm, at which wavelength the adducts showed intense absorbance, unlike their precursors or decomposition products. Reactions with substrates were studied using the double-mixing mode of the stopped-flow instrument. In these experiments, the solutions of the diiron(II,II) precursor (**1**) and O_2 were combined at low temperature in the first mixing chamber, incubated for the time required to obtain the maximum yield of the adduct **2**, and then combined with a solution of substrate at the same low temperature in the second mixing cell.

Batch Reaction of 2-THF with PPh_3. Dry O_2 was bubbled through a solution of $[(dxlCO_2)_4Fe_2(THF)_2]$ (**1-THF**) (50.0 mg, 2.62×10^{-5} mol) in CH_2Cl_2 (5 mL) at 203 K for 15 min, causing the yellow solution to turn deep red-brown. The headspace of the flask was evacuated and purged with N_2 three times, and then, Ar was bubbled through the solution for 25 min. A solution of PPh_3 (13.5 mg, 5.15×10^{-5} mol, slightly less than 2 equiv based on **2-THF**) in CH_2Cl_2 (0.5 mL) was added, causing a color change to paler green-brown. This solution was stirred for 15 min at 203 K, and then, 2 mL of NH_3(aq) (28−30%, Aldrich) was injected, resulting in a color change to orange. This solution was stirred and warmed to room temperature for 30 min. The organic layer was then separated, the aqueous layer was washed with CH_2Cl_2 (2×10 mL), and the organic fractions were combined and dried over Na_2SO_4. The solvent was removed under reduced pressure. A portion of $PMes_3$ (7.6 mg, 1.96×10^{-5} mol) was added to the residue as a standard, and the entire sample was then dissolved in $CDCl_3$ for quantitiative analysis by $^{31}P\{^1H\}$ NMR spectroscopy: (121.5 MHz) δ 30.92 ($OPPh_3$), −4.89 (PPh_3), −35.92 ($PMes_3$) ppm. On the basis of integration versus the internal standard, $PMes_3$, the ratio $OPPh_3$/PPh_3 was ∼1:1, with an 80% recovery of products based on the amount of PPh_3 added, corresponding to a $OPPh_3$ yield of 80% based on the amount of **1-THF** used in the reaction. In a control experiment, the entire procedure was repeated, except no **1-THF** was used. In this case, 70% of the added PPh_3 was recovered, and only 4% conversion to $OPPh_3$ was observed (on the basis of **1-THF**). In a third experiment, $^{18}O_2$ was used to prepare **2-THF**, and the product mixture was analyzed by mass spectrometry. The $OPPh_3$ contained ∼90% ^{18}O, confirming that the O-atom transferred to PPh_3 derived from O_2.

Acknowledgment. We thank the NSF (CHE0111202 to E.V.R.-A.), the Research Corporation (RI0223 to E.V.R.-A.), the University of Minnesota (Louise T. Dosdall fellowship to A.M.R.), and the NIH (GM38767 to L.Q.) for financial support. In addition, we thank Prof. David Blank for helpful discussions and Charlotte Williams for some experimental support.

Supporting Information Available: Eyring plot for the decomposition of **2-Py** in the absence of added substrate (Figure S1) and second-order rate constants for the oxygenation of diferrous complexes **1** determined at 233 K (Table S1). This material is available free of charge via the Internet at http://pubs.acs.org.

IC049976T